

Atmospheric Response to Arctic and Antarctic Sea Ice: The Importance of Ocean–Atmosphere Coupling and the Background State

DOUG M. SMITH, NICK J. DUNSTONE, ADAM A. SCAIFE, EMMA K. FIEDLER, DAN COPSEY, AND STEVEN C. HARDIMAN

Met Office Hadley Centre, Exeter, United Kingdom

(Manuscript received 1 August 2016, in final form 16 December 2016)

ABSTRACT


The atmospheric response to Arctic and Antarctic sea ice changes typical of the present day and coming decades is investigated using the Hadley Centre global climate model (HadGEM3). The response is diagnosed from ensemble simulations of the period 1979 to 2009 with observed and perturbed sea ice concentrations. The experimental design allows the impacts of ocean–atmosphere coupling and the background atmospheric state to be assessed. The modeled response can be very different to that inferred from statistical relationships, showing that the response cannot be easily diagnosed from observations. Reduced Arctic sea ice drives a local low pressure response in boreal summer and autumn. Increased Antarctic sea ice drives a poleward shift of the Southern Hemisphere midlatitude jet, especially in the cold season. Coupling enables surface temperature responses to spread to the ocean, amplifying the atmospheric response and revealing additional impacts including warming of the North Atlantic in response to reduced Arctic sea ice, with a northward shift of the Atlantic intertropical convergence zone and increased Sahel rainfall. The background state controls the sign of the North Atlantic Oscillation (NAO) response via the refraction of planetary waves. This could help to resolve differences in previous studies, and potentially provides an “emergent constraint” to narrow the uncertainties in the NAO response, highlighting the need for future multimodel coordinated experiments.

1. Introduction

Over the last three and a half decades Arctic sea ice extent has declined substantially, at an average rate of around 4% per decade annually and more than 10% per decade during the summer (e.g., Vaughan et al. 2013). Further reductions are expected as the climate continues to warm, with model projections suggesting that perennial Arctic sea ice could disappear within the next few decades (e.g., Collins et al. 2013). In contrast, Antarctic sea ice extent has increased slightly, at a rate of about 1.5% decade⁻¹, but is projected to decrease in future (Vaughan et al. 2013; Collins et al. 2013). Sea ice plays a key role in modulating the flow of energy in the climate system, with potentially important impacts on the global atmospheric circulation. Quantifying and understanding

the influence of sea ice changes on the atmospheric circulation is therefore crucial for predicting how climate will change in the coming decades.

Many studies have investigated the potential influence of sea ice on the atmospheric circulation, and are summarized in recent review papers (Cohen et al. 2014; Vihma 2014; Walsh 2014; Barnes and Screen 2015; Overland et al. 2015). Of particular interest is whether Arctic sea ice reductions could affect the North Atlantic Oscillation (NAO), and hence the winter climate in Europe, North America, and parts of Asia. However, there is no consensus even on the sign of the NAO response: previous modeling studies simulate a full spectrum of responses including negative NAO (Honda et al. 2009; Seierstad and Bader 2009; Mori et al. 2014; Kim et al. 2014; Deser et al. 2015; Nakamura et al. 2015), positive NAO (Singarayer et al. 2006; Strey et al. 2010; Orsolini et al. 2012; Rinke et al. 2013; Cassano et al. 2014; Screen et al. 2014), little response (Screen et al. 2013; Petrie et al. 2015; Blackport and Kushner 2016), and a response that depends on the details of the forcing (Alexander et al. 2004; Petoukhov and Semenov 2010;

 Denotes content that is immediately available upon publication as open access.

Corresponding author: Doug Smith, doug.smith@metoffice.gov.uk

Peings and Magnusdottir 2014; Sun et al. 2015; Pedersen et al. 2016). In contrast, the atmospheric response to Antarctic sea ice has received less attention (Simmonds and Budd 1991; Simmonds and Wu 1993; Menéndez et al. 1999; Kidston et al. 2011; Bader et al. 2013).

Recent studies have highlighted the importance of ocean–atmosphere coupling for simulating the response to sea ice (Deser et al. 2015, 2016; Tomas et al. 2016). However, the response to other forcings, including greenhouse gases, ozone, changes in the polar vortex, and Atlantic sea surface temperatures, is known to depend on the climatological background state (Son et al. 2010; Kidston and Gerber 2010; Sigmund and Scinocca 2010; Garfinkel et al. 2013; Omrani et al. 2014), but this has not previously been investigated in relation to sea ice. Here we report on a comprehensive set of modeling experiments that are designed to assess the influences of both coupling and background state on the response to sea ice. We find that both are important. Coupling generally amplifies the atmospheric response because sea surface temperature (SST) changes driven by sea ice can spread to the surrounding ocean and are consequently larger. The coupled SST response reaches the tropics, and influences Sahel rainfall. The background state plays a key role in the NAO response to reduced Arctic sea ice in our model, to the extent that the sign of the NAO response is controlled by the refraction of planetary waves by the climatological flow. This provides a potential “emergent constraint” to narrow the uncertainties in the NAO response, highlighting the need for multimodel coordinated experiments.

The manuscript is organized as follows. Section 2 describes the model and experimental design, with results presented in section 3. Sections 4 and 5 explore the boreal winter NAO response and in particular why it depends on the background state. In section 6 we investigate a potential emergent constraint to reduce the uncertainties in the NAO response, and in section 7 we show that the response cannot be inferred from statistical relationships, highlighting the need for model experiments. We summarize and present conclusions in section 8.

2. Model and experimental design

We assess the impact of Arctic and Antarctic sea ice variations on the climate system by performing numerical experiments using the Met Office Hadley Centre global climate model HadGEM3, at the global configuration GA3 (Walters et al. 2011). The atmosphere resolution is 1.875° longitude by 1.25° latitude (approximately 130 km in midlatitudes), with 85 vertical levels and an upper boundary at 85 km providing a realistic

simulation of the stratosphere (Hardiman et al. 2012). We perform experiments with both an atmosphere only model forced by sea surface temperatures and sea ice concentrations at the lower boundary (following the Atmosphere Model Intercomparison Project protocol, hereafter AMIP), and a fully coupled atmosphere ocean model (hereafter CPLD) but with constrained sea ice concentrations (described below). The ocean component of the coupled model is NEMO3.2 with 75 vertical levels (1 m thick at the surface increasing to approximately 200 m at a depth of 6000 m) and a horizontal resolution of 1° longitude by 1° latitude increasing to 0.3° latitude in the tropics. Note that because CPLD SSTs are unconstrained we use time-varying SSTs in AMIP rather than climatological monthly averages to avoid suppressing the interannual SST variability in AMIP relative to CPLD.

To assess the impact of sea ice changes we perform two sets of simulations of the 30-yr period from December 1979 to November 2009. In the first (control) set the model is provided with the observed monthly mean fields of Arctic and Antarctic sea ice concentration (Hurrell et al. 2008). In the second (perturbed sea ice) set, the model is constrained by perturbed monthly mean fields of sea ice concentration, where the perturbations are designed to investigate changes typical of the present day and coming decades rather than the much larger changes expected toward the end of the century. Over the Arctic the perturbed sea ice concentrations for each month are obtained by eroding the ice edge until the Northern Hemisphere total sea ice area is consistent with that expected by projecting the observed monthly trends in Northern Hemisphere total sea ice area forwards. The observed trends are computed over the final 15 years of our period (1994–2009). Specifically, we require a continuous 30-yr time series of perturbed monthly mean sea ice concentration fields in order to repeat the simulations of the period 1979–2009. This is created by starting from the 5-yr averaged monthly fields from the end of our period (2005–09) and then gradually eroding the sea ice edge at all longitudes until the total area is consistent with the projected trend of total area at the required time. This approach attempts to simulate the gradual melting of the ice pack expected over the coming 30 years, and avoids holes in the ice pack that could appear if we simply projected the trends forwards at each grid point. We originally did not intend to perturb Antarctic sea ice, but we inadvertently created perturbed ice fields equal to the 5-yr averaged monthly fields from the end of our period (2005–09). Although this was unintentional, it does provide an opportunity to investigate the influence of Antarctic sea ice anomalies typical of the present day.

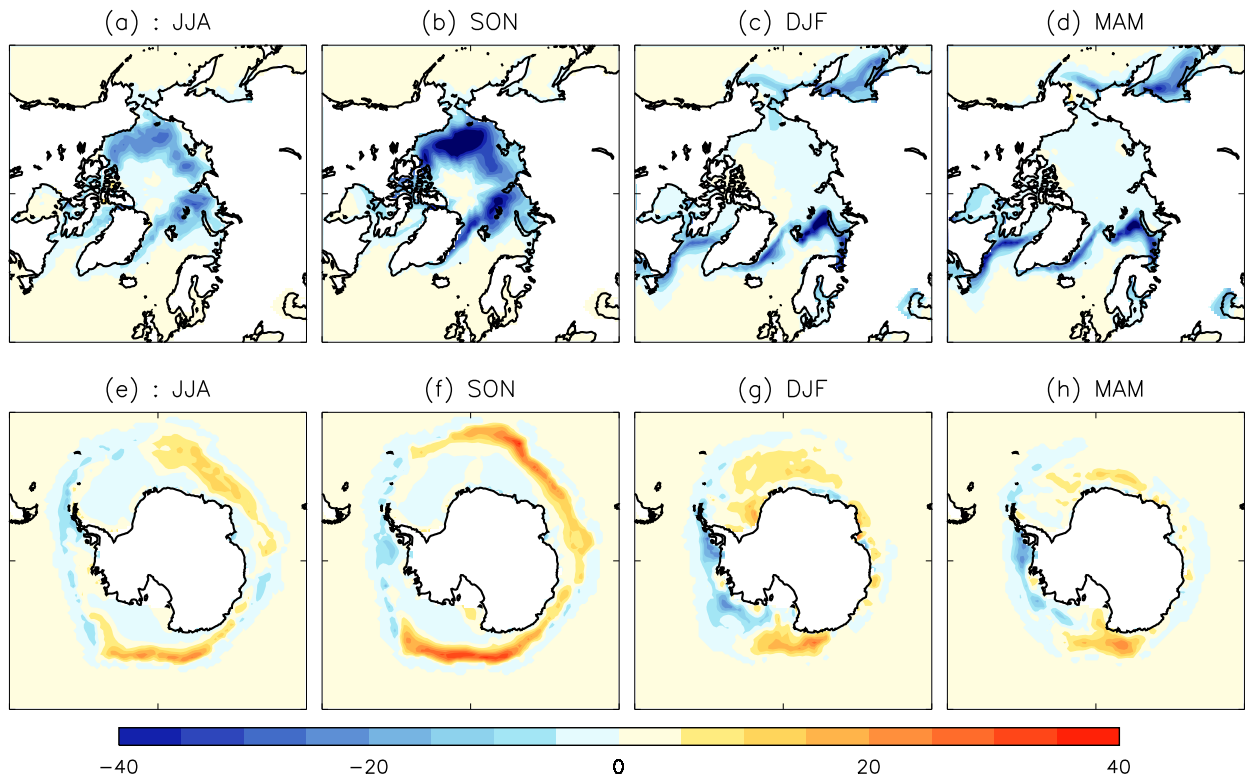


FIG. 1. Imposed seasonal mean sea ice concentration difference (%) in (top) the Arctic and (bottom) the Antarctic, during (a),(e) JJA, (b),(f) SON, (c),(g) DJF, and (d),(h) MAM. Differences are averaged over all 30 years.

For the AMIP experiments the observed or perturbed sea ice concentrations are supplied at the lower boundary along with observed monthly mean fields of SST (Hurrell et al. 2008). The SSTs are identical in the control and perturbed sea ice experiments except where the sea ice has disappeared. In these regions the SST for the perturbed experiments is set to 273.14 K (linearly interpolating from 271.36 K based on the sea ice fraction). These values were chosen by analyzing observed SSTs at the sea ice edge. Specifically, grid points close to the ice edge were found to have an average temperature of 273.14 K, becoming progressively colder toward the freezing point of seawater (271.36 K) as the sea ice fraction increased. For the CPLD experiments the observed or perturbed sea ice conditions are imposed during the coupled model integration by relaxing to the required sea ice concentrations (interpolated to the appropriate time from the adjacent monthly mean values), using a 6-h relaxation time scale. This technique is the same as that used to create sea ice initial conditions for the Met Office decadal prediction system (DePreSys; Smith et al. 2013). To avoid undesired responses in deep ocean currents including the Atlantic meridional overturning circulation that might be driven by persistent relaxation increments (Dunstone and

Smith 2010), we constrain ocean temperature and salinity below 200 m by relaxing to monthly mean values from the Met Office Statistical Ocean Reanalysis (MOSORA; Smith et al. 2015). Our experiments are therefore similar to slab ocean experiments (Deser et al. 2015, 2016) but potentially simulate dynamical responses in the upper ocean. However, our experiments are unsuitable for studying potential influences of sea ice on deep ocean circulation that could be important on decadal or longer time scales.

We perform both AMIP and CPLD experiments in order to investigate the role of ocean–atmosphere coupling, which has been found to be important in simulating the response to sea ice (Deser et al. 2015, 2016; Tomas et al. 2016). However, differences between CPLD and AMIP could also be caused by differences in the climatological background state of the model, because SSTs in the AMIP simulations are close to reality whereas the CPLD experiments are only constrained below 200 m so that SSTs may drift toward the coupled model biases. To isolate the impact of the background state we perform an additional set of experiments (hereafter AMIP_CPLD) by repeating the AMIP simulations (both control and perturbed) but imposing the SST biases from the CPLD simulations. This is achieved

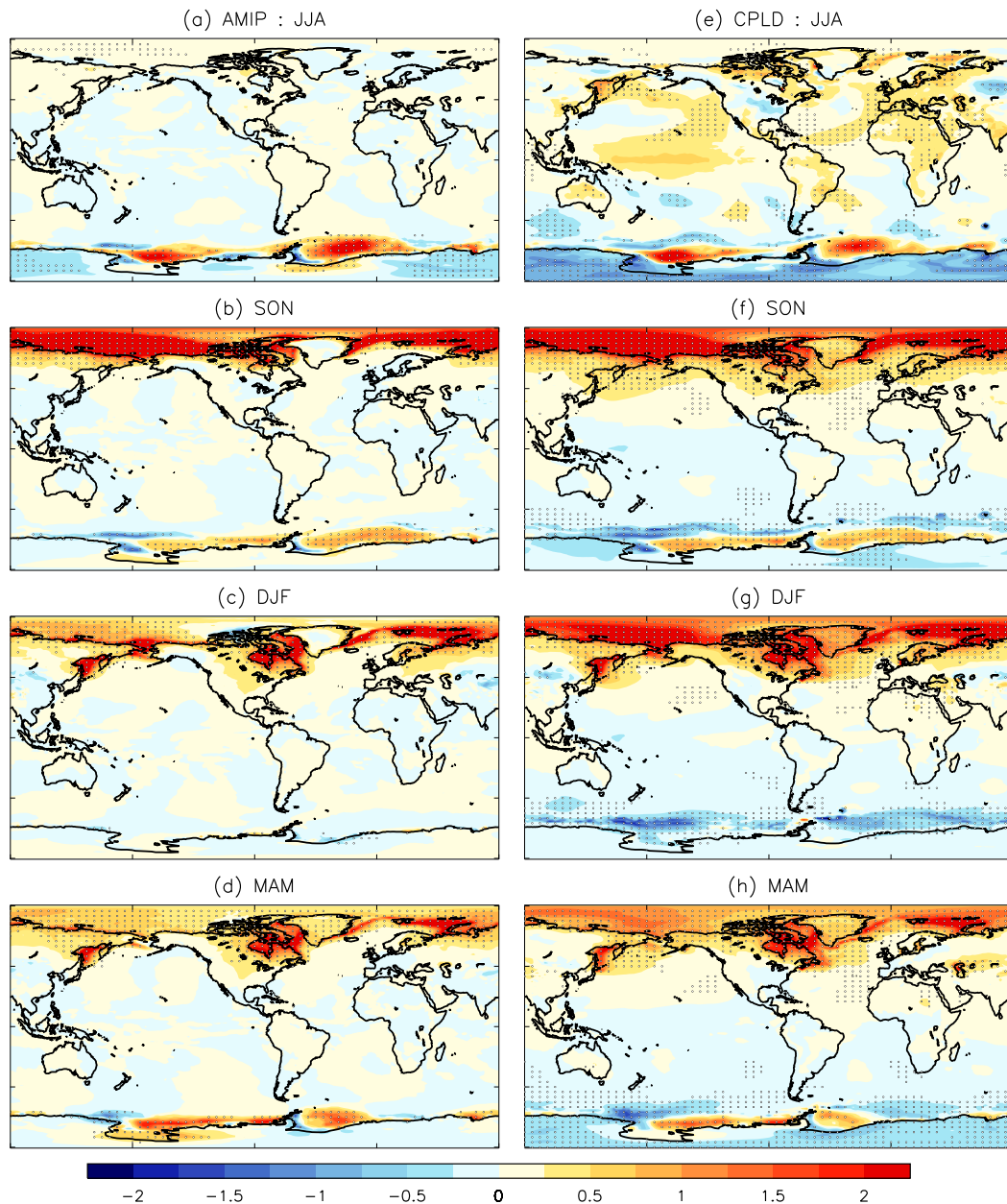


FIG. 2. Seasonal near-surface temperature difference ($^{\circ}\text{C}$) between reduced ice and control simulations in (a)–(d) AMIP and (e)–(h) CPLD experiments. Differences are averaged over all 30 years and all ensemble members, with stippling showing where values are significant at the 95% level based on a two-tailed Student's t test.

by removing at each grid point and month the observed climatological average SST and replacing it with the climatological average from the ensemble mean of the CPLD experiments, thereby superimposing the observed variability onto the CPLD background state. The changes in sea ice concentration and SST where the sea ice has disappeared are the same as in the AMIP experiment.

Both control and perturbed sea ice simulations consist of multiple ensemble members in order to isolate the impact of sea ice changes that appears to be small relative to intrinsic variability in models (e.g., Screen et al. 2013; Mori et al. 2014). However, we note that the signal-to-noise ratio may be too small in models (Eade et al. 2014; Scaife et al. 2014; Dunstone et al. 2016) so that the magnitude of any response could be underestimated.

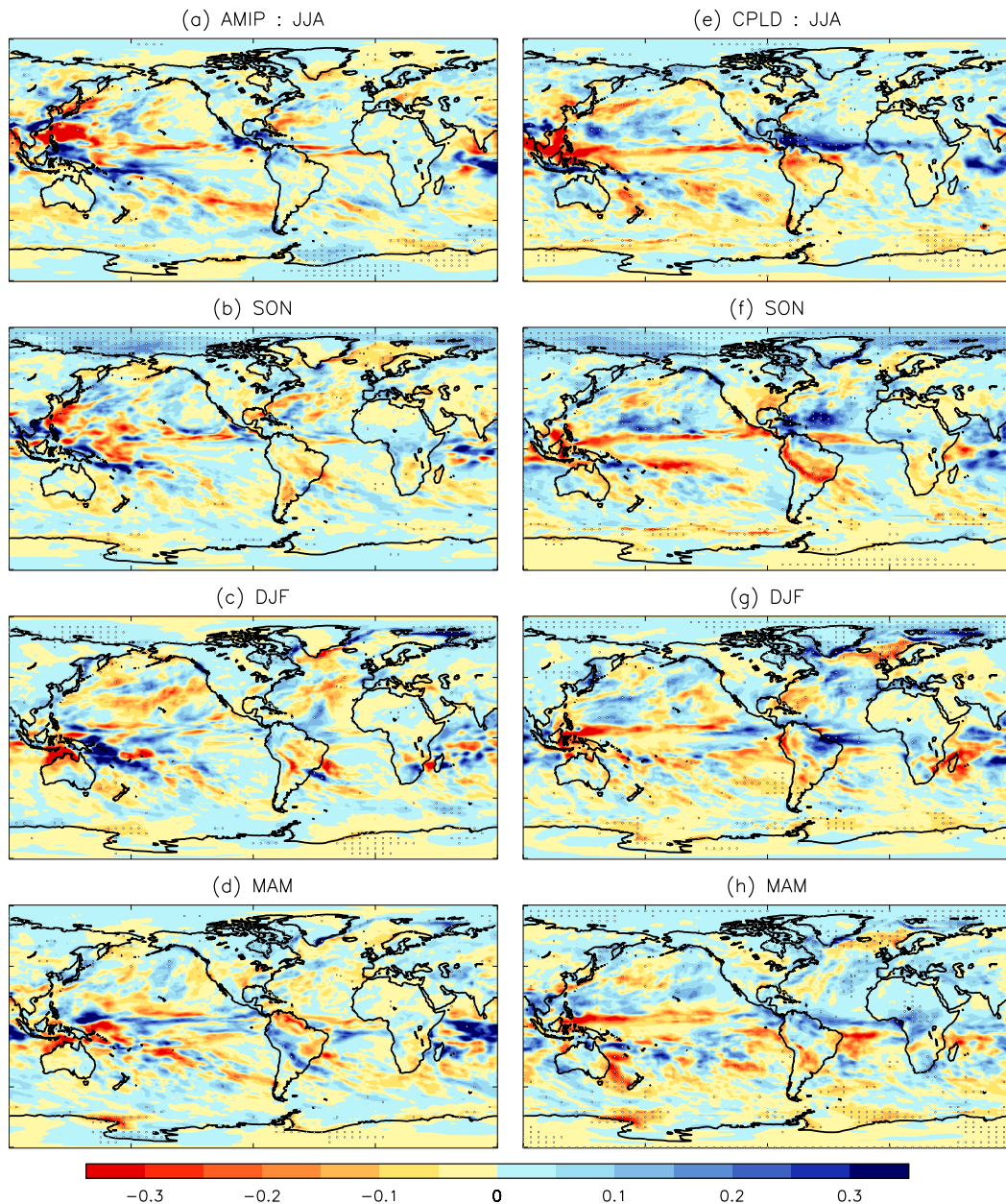


FIG. 3. As in Fig. 2, but for precipitation rate (mm day^{-1}).

Hence we focus on diagnosing, and understanding, the robust response in our model. The AMIP and CPLD simulations contain 10 ensemble members (a total of 300 simulated years) and the AMIP_CPLD simulation contains 5 ensemble members. Ensemble members were generated by very small perturbations to the SST initial conditions. We diagnose the impact of sea ice as the difference between the perturbed sea ice and control experiments, and compute the average difference over all 30 years and all ensemble members to obtain the most robust results. Results are presented for the different

seasons: June–August (JJA), September–November (SON), December–February (DJF), and March–May (MAM). We test for statistical significance using a two-tailed Student's t test of the difference between two means.

3. Results

The imposed sea ice concentration perturbations averaged over the whole 30-yr period are shown in Fig. 1. Arctic sea ice is reduced in all seasons, with the largest

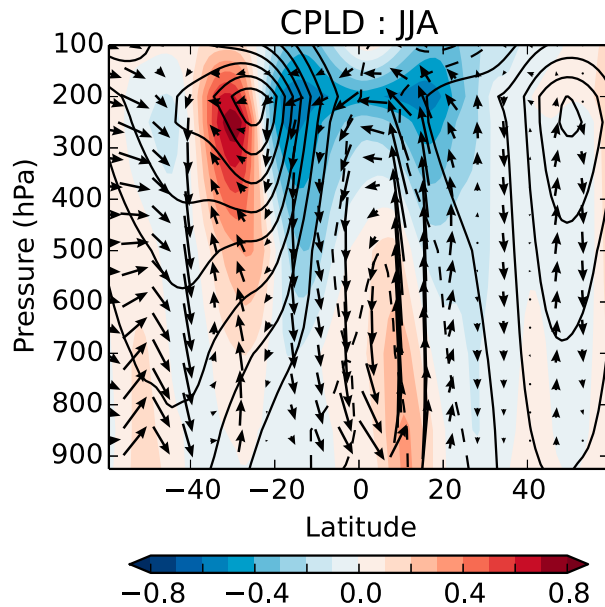


FIG. 4. Cross section showing JJA tropospheric circulation response in the Atlantic simulated by CPLD as a function of latitude and height (pressure). Colors show the zonal wind response (m s^{-1}); vectors represent the meridional and vertical wind response (where vertical wind is the pressure velocity multiplied by minus one). Values are zonally averaged over the region 80° to 20°W . Contours show the climatological zonal winds (contour interval 5 m s^{-1} ; negative contours are dashed). The lower level is 1000 hPa.

reductions, especially in the interior of the ice pack, in boreal summer and autumn, and reductions mainly confined to the marginal ice regions in winter and spring. Antarctic sea ice is mainly increased, especially in June to November when the seasonal extent is largest, reflecting an increasing trend over the last few decades (e.g., Vaughan et al. 2013). However, there is some reduction around the Antarctic Peninsula.

Near-surface temperatures (Fig. 2) warm (cool) in the cold seasons where sea ice is reduced (increased), consistent with reduced ocean to atmosphere heat fluxes in the presence of sea ice (e.g., Screen et al. 2013; Peings and Magnusdottir 2014; Deser et al. 2015). There is little temperature change in the summer months in AMIP (Figs. 2a,c) since the imposed SST where the ice has been removed is similar to the control run surface temperature over sea ice, which is governed by temperatures near the melting point at this time of year. Temperature changes are larger in CPLD than AMIP, consistent with other studies (Deser et al. 2015, 2016), because areas of sea ice loss warm in summer, potentially leading to surface warming into the colder seasons, and also because changes over the sea ice are able to spread to the surrounding ocean in CPLD. The active ocean in CPLD also enables remote changes in SST (Deser et al. 2015; Chiang and Bitz

2005). In particular, we find a warming in the tropical Atlantic in JJA, which will be discussed further below.

Both AMIP and CPLD show a significant increase in precipitation over the Arctic in SON (Fig. 3), consistent with increased evaporation in the absence of sea ice (not shown). However, precipitation changes over mid-latitude land regions are insignificant and hypothesized increases in Eurasian snow cover (Cohen et al. 2012) are not simulated by our model (not shown).

The CPLD experiments simulate warming in the North Atlantic in response to reduced Arctic sea ice in all seasons, projecting onto the positive phase of Atlantic multidecadal variability (e.g., Knight et al. 2005). The warming reaches the tropics especially in JJA and to a lesser extent SON (Figs. 2e,f), driving an anomalous Hadley circulation (Fig. 4; Chiang and Bitz 2005, Kang et al. 2008; Dunstone et al. 2011) and a northward shift of the Atlantic intertropical convergence zone (ITCZ) especially on the western side of the basin (Figs. 3e,f). Although the changes in zonal wind are small and generally not significant for individual grid points, there is a reduction in zonal wind shear averaged over the hurricane main development region (MDR; 10° – 20°N , 80° – 20°W) of 0.6 m s^{-1} ($p < 0.07$), amounting to 15% of the interannual variability. Reduced zonal wind shear and increased ascent in the MDR (Fig. 4) would be expected to promote hurricanes (e.g., Goldenberg et al. 2001; Smith et al. 2010; Dunstone et al. 2011), but the magnitude of this response is difficult to quantify in a model that does not have sufficiently high resolution to simulate realistic hurricanes. An anomalous Hadley circulation is also associated with Sahel rainfall (Sheen et al. 2017), which significantly increases in CPLD (0.09 mm day^{-1} , $p < 0.025$, computed over the region 10° – 20°N , 20°W – 35°E for the peak rainfall period July–September), comparable in magnitude to long-term projections (Biasutti 2013). These responses in the tropical Atlantic are not simulated by AMIP, showing the need for coupled models to simulate the full response to sea ice changes in agreement with previous studies (Deser et al. 2015, 2016; Tomas et al. 2016). However, we note that our experiments inhibit changes in deep ocean circulation that could also play a role, especially on decadal time scales.

Changes in mean sea level pressure (MSLP) are shown in Figs. 5 and 6 for the Arctic and Antarctic regions. The AMIP simulations show a weak low pressure over reduced Arctic sea ice in all seasons consistent with a “heat low” (e.g., Racz and Smith 1999) response to surface warming (although significant changes are not evident over all regions of reduced sea ice, especially in JJA). The CPLD simulations also show lower pressure in JJA and SON. The response is larger in magnitude

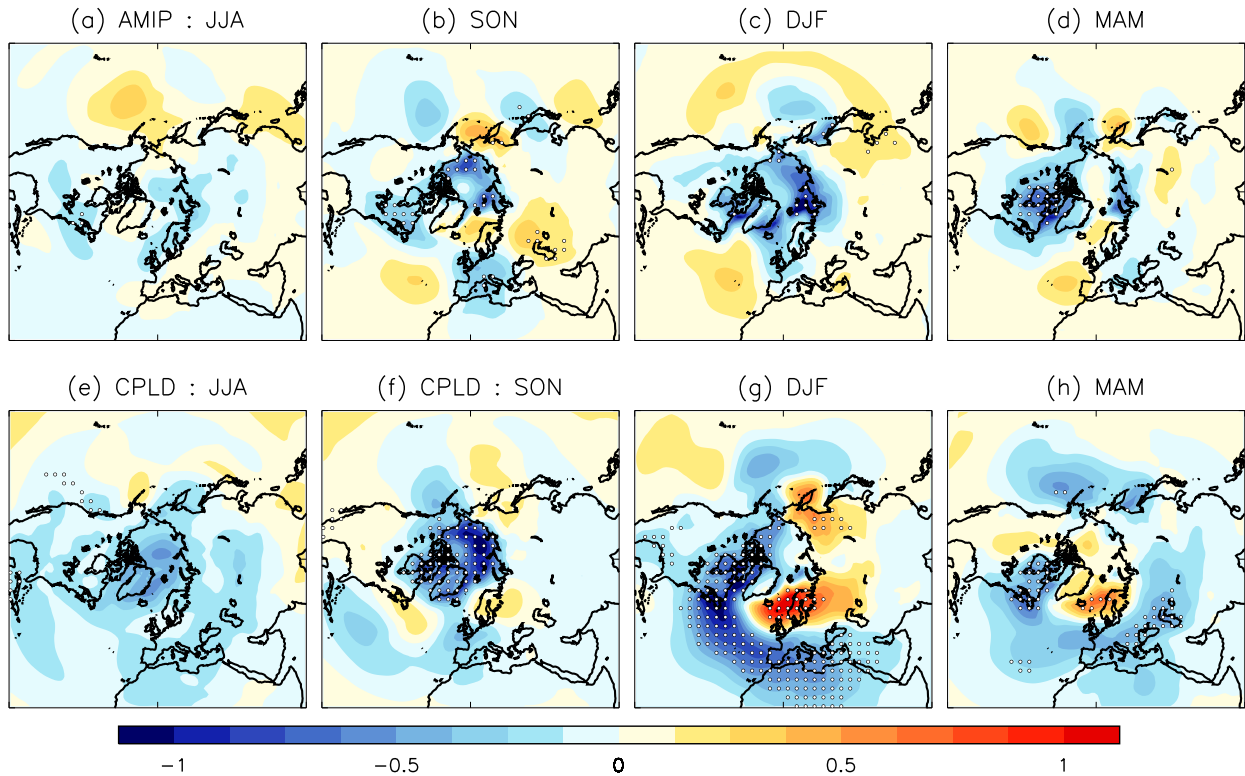


FIG. 5. As in Fig. 2, but for Northern Hemisphere mean sea level pressure (hPa).

than AMIP since the surface warms more (Fig. 2) and is significant for the area average north of 60°N in both seasons. In boreal winter the AMIP response projects onto a significant positive North Atlantic Oscillation [NAO; computed here as the difference between normalized pressure indices for Lisbon (38.7°N , 9.1°W) and Iceland (65.1°N , 22.7°W)] (Hurrell 1995). However, the NAO response is baroclinic, with no significant response in 500-hPa geopotential height ($z500$) over the Arctic (not shown). In contrast, the CPLD simulations are very different in boreal winter and spring, showing a barotropic response with significantly high $z500$ over the Arctic (not shown), high pressure over the Nordic Seas, and low pressure farther south, and hence a significant negative NAO. We focus on the DJF NAO and investigate the reason for the different responses in CPLD and AMIP in sections 4 and 5. Over the Antarctic the response broadly resembles a positive southern annular mode (SAM; the difference in normalized zonal mean pressure between 40° and 65°S ; Gong and Wang 1999), with low pressure near the pole surrounded by a ring of high pressure. However, the SAM response is only significant in MAM in CPLD and JJA in AMIP.

Zonal mean changes as a function of latitude and height are shown in Figs. 7 and 8 for temperature and

zonal wind. In AMIP, DJF warming over the Arctic is confined to the boundary layer, due to the surface-based warming and the stable lower atmosphere during winter. Consequently there is very little response in zonal wind (Figs. 7c and 8c) consistent with little change in MSLP (Fig. 5c). In contrast, CPLD shows a barotropic response with a weakening of the stratospheric polar vortex and weaker zonal winds extending down to the surface (Fig. 8g). Furthermore, the upper troposphere and stratosphere warm (Fig. 7g), consistent with adiabatic warming due to descent and compression of air over the pole leading to high pressure and hence a negative NAO (Fig. 5g).

Both AMIP and CPLD simulate a poleward shift of Southern Hemisphere midlatitude tropospheric jet in the cold seasons (JJA and SON) in response to increased Antarctic sea ice extent consistent with previous studies (Simmonds and Budd 1991; Simmonds and Wu 1993; Menéndez et al. 1999; Kidston et al. 2011; Bader et al. 2013). The mechanism involves changes in planetary waves (not shown), in agreement with Kidston et al. 2011, and is the same as for the CPLD NAO response that is discussed in section 5. Strengthened Southern Hemisphere winds in MAM are simulated by CPLD but not AMIP (Figs. 8d,h). This is discussed further in the next section.

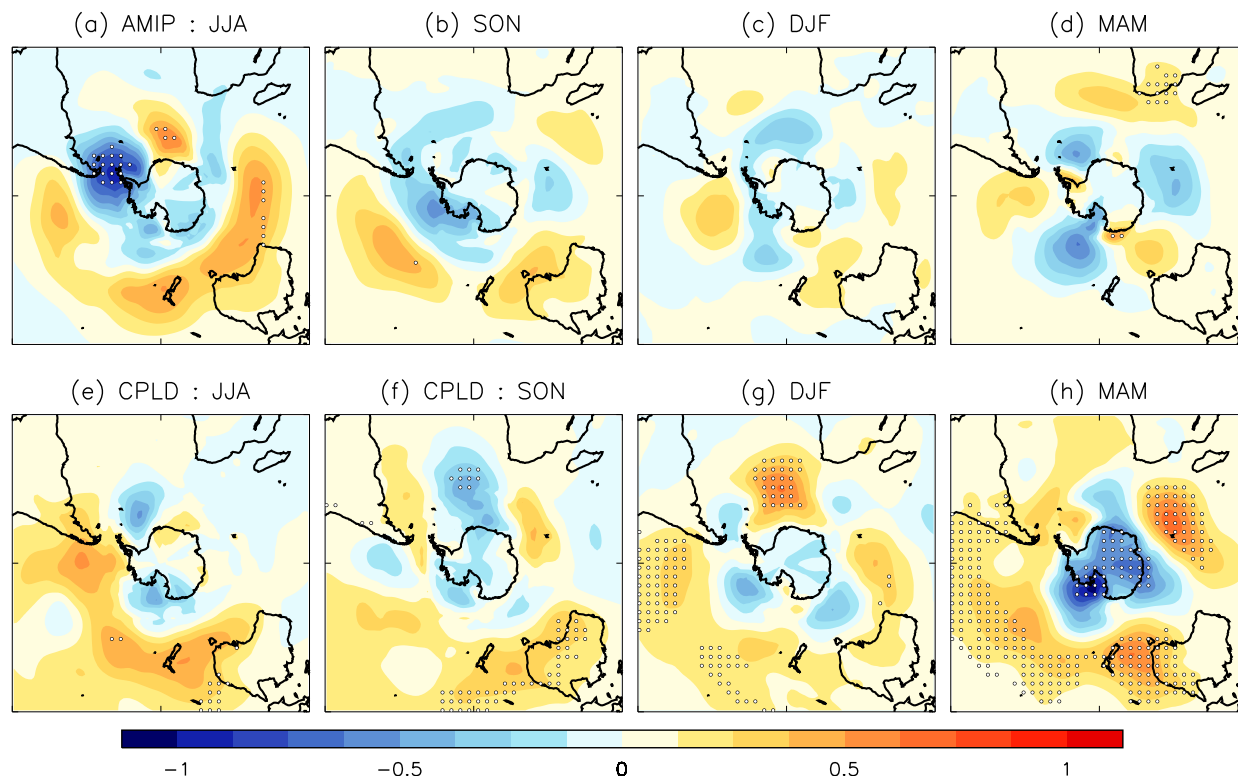


FIG. 6. As in Fig. 2, but for Southern Hemisphere mean sea level pressure (hPa).

4. Why is the NAO response different in CPLD and AMIP?

We now investigate the reasons for the different DJF-mean NAO response in AMIP and CPLD. Whether reduced Arctic sea ice induces a positive or negative NAO has important implications for wintertime weather and climate over Europe, the United States, and Asia. However, there is no consensus in previous studies even on the sign of the NAO response, as summarized in section 1. In our experiments the NAO response depends on whether the model was run in AMIP or CPLD mode (cf. Figs. 5c,g). Understanding the reason for this may help to resolve the lack of agreement in previous studies.

Two possible causes of differences between AMIP and CPLD are 1) ocean–atmosphere coupling, which allows sea ice changes to influence the surrounding ocean in CPLD and enables feedbacks between the atmosphere and the active upper ocean, and 2) differences in the climatological background state, which arise because AMIP SSTs are constrained to be close to reality whereas the upper 200 m of our CPLD simulations are free to drift toward the coupled model’s preferred state. Differences in the background state are illustrated in Fig. 9 for DJF. The CPLD simulations are cooler than AMIP in most regions but warmer in the Southern

Ocean. The tropospheric jets (at around 200 hPa) are weakened and shifted poleward in both hemispheres, and the northern stratospheric polar vortex is strengthened and shifted poleward.

We isolate the impact of background state using the AMIP_CPLD simulations. These repeat AMIP with the same SST and sea ice perturbations, but imposing the climatological background ocean state from CPLD (as described in section 2). This successfully reproduces the CPLD biases in zonal wind (cf. Figs. 9b,c). The AMIP_CPLD simulations closely reproduce the CPLD DJF Northern Hemisphere MSLP response (cf. Figs. 10a and 5g), together with the weakened zonal winds throughout the troposphere and stratosphere (cf. Figs. 10c and 8g). This shows that background state rather than other effects of coupling is the main reason for differences in the NAO response between AMIP and CPLD. However, the AMIP_CPLD simulations do not reproduce the CPLD MAM MSLP response over the Antarctic (cf. Figs. 10b and 6h) or the strengthened Southern Hemisphere winds (cf. Figs. 10d and 8h), showing that coupling (such as the stronger cooling shown in Fig. 2h) is important here.

How can the NAO response to the same sea ice changes be opposite in the AMIP and CPLD experiments? A possible explanation is that the total response

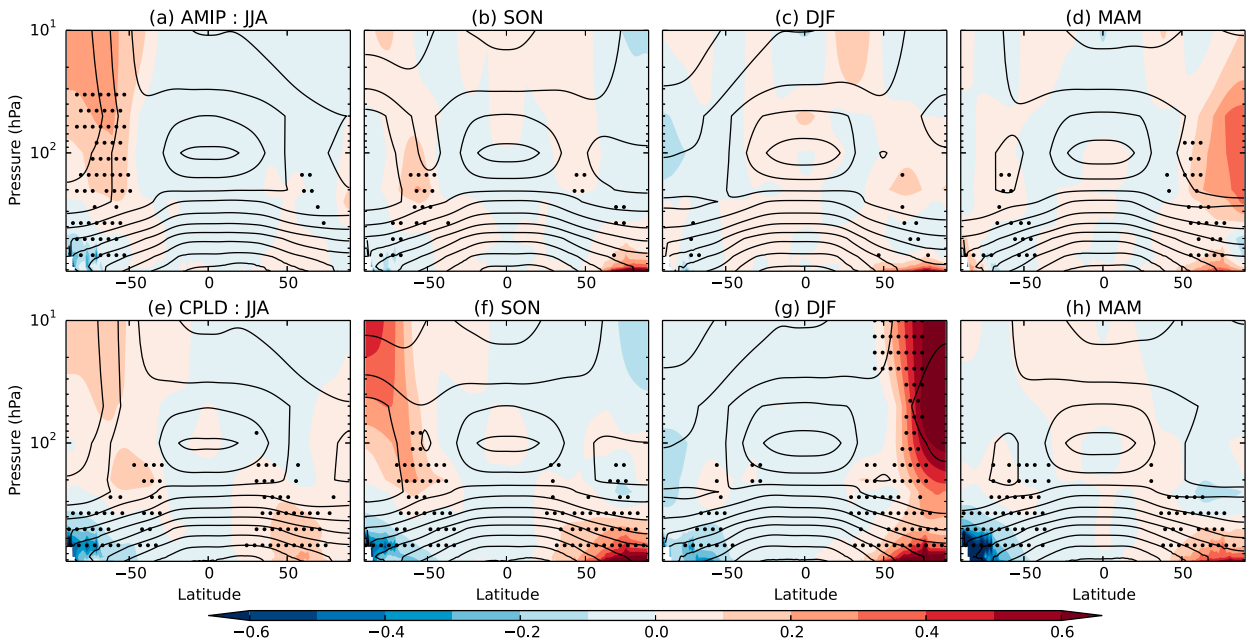


FIG. 7. As in Fig. 2, but for zonal mean temperature ($^{\circ}\text{C}$) as a function of latitude and height (in pressure coordinates). Contours show the climatological temperatures (contour interval 10°C).

is a combination of thermodynamic and dynamic responses (e.g., Deser et al. 2004). The thermodynamic response consists of low pressure (a heat low) over the warmer surface temperatures where the sea ice has been reduced, and hence a positive NAO. In contrast, the

dynamic response consists of a weakening of the mid-latitude westerly winds, with a weaker meridional pressure gradient to maintain geostrophic balance and higher pressure over polar regions as seen in a negative NAO. We suggest that the thermodynamic response is

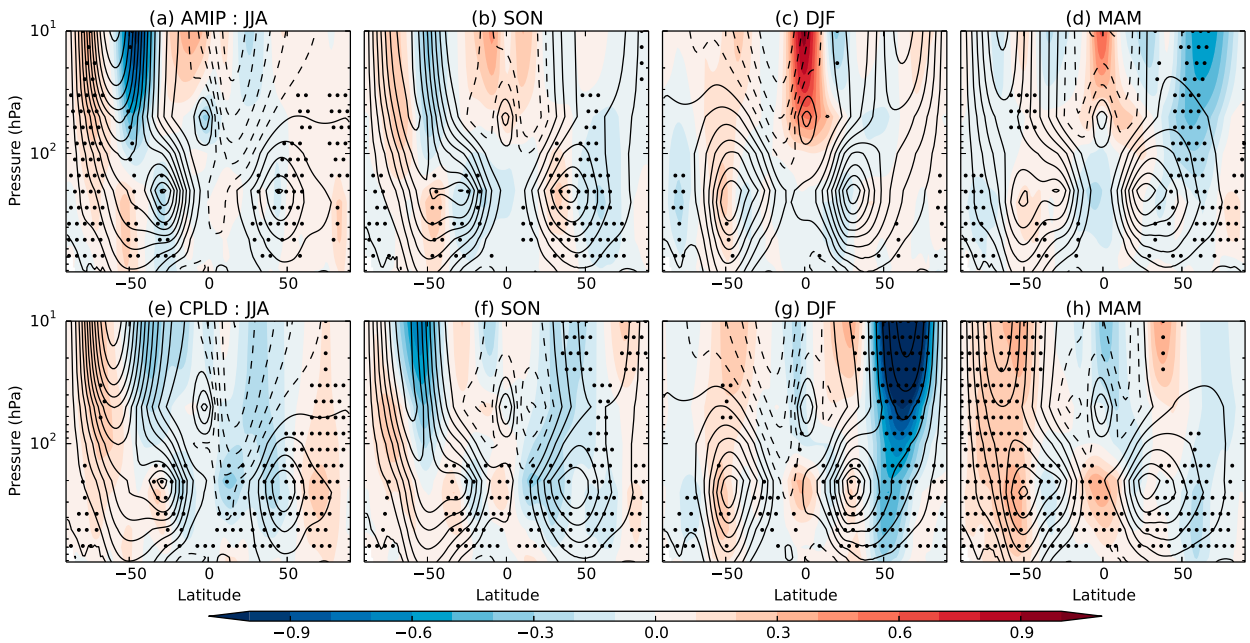


FIG. 8. As in Fig. 2, but for zonal mean zonal velocity (m s^{-1}) as a function of latitude and height (in pressure coordinates). Contours show the climatological zonal winds (contour interval 5 m s^{-1} ; negative contours are dashed).

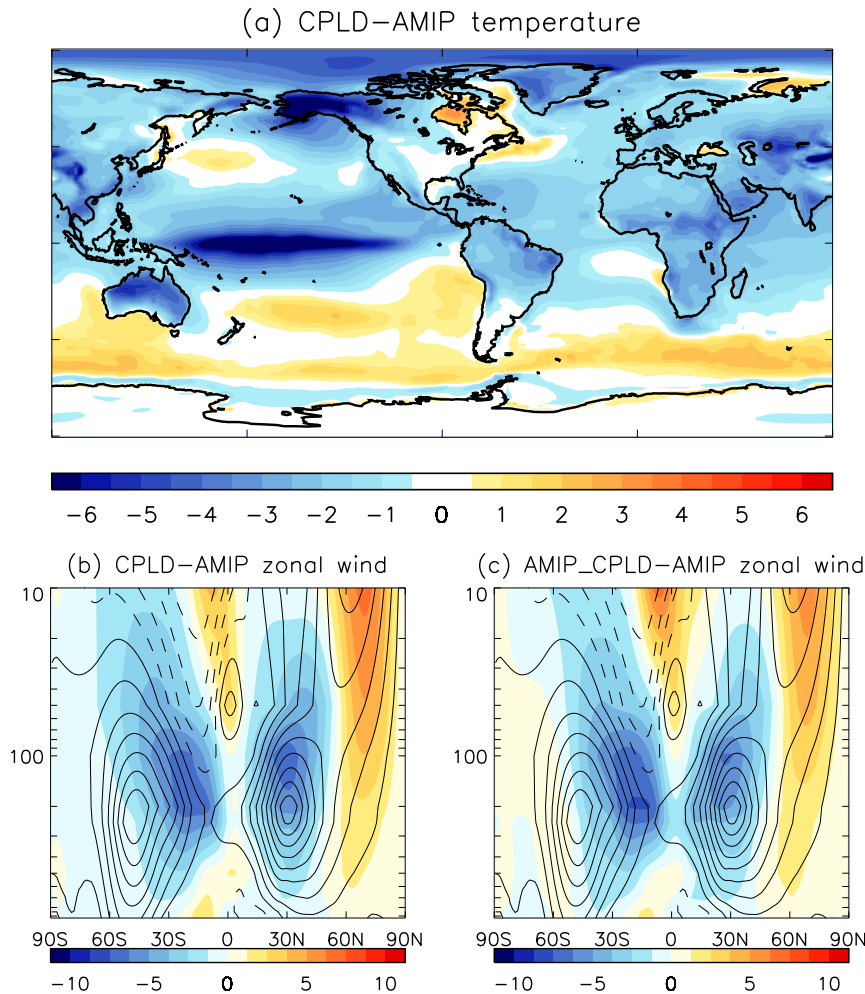


FIG. 9. Climatological difference between CPLD and AMIP (a) near-surface temperature and (b) zonal mean zonal wind as a function of latitude and height (hPa). (c) As in (b), but for the difference between AMIP_CPLD and AMIP. Differences are shown for DJF averaged over all 30 years of the control experiments. Contours show the AMIP climatological winds (contour interval 5 m s^{-1} ; negative contours are dashed).

dominant in AMIP, whereas the dynamic response is dominant in CPLD, leading to opposite responses in the NAO. However, the AMIP simulations do show a weakening of the midlatitude westerly winds in MAM (Fig. 8d), suggesting that a dynamic response is occurring but is delayed relative to CPLD and AMIP_CPLD.

5. Why does the NAO response depend on the background state?

Although AMIP_CPLD successfully reproduces the large scale patterns of bias in the CPLD background state (Figs. 9b,c), the magnitudes of the biases are slightly smaller. This provides an opportunity to investigate the response across the three sets of simulations with different background states (AMIP, CPLD,

and AMIP_CPLD) in order to understand the physical reasons for their differences. We present results focusing on the DJF Atlantic eddy-driven jet (diagnosed from zonal velocity at 200 hPa, 50° – 60° N, 60° – 0° W), but results for the polar vortex (at 10 hPa, 60° N) provide similar conclusions.

Model responses to changes in ozone (Son et al. 2010), greenhouse gases (Kidston and Gerber 2010), and the stratospheric polar vortex (Garfinkel et al. 2013) depend on the climatological position of the jet. We find a similar dependence for the response of the Atlantic jet to Arctic sea ice (Fig. 11a). One possibility is that the influence of the sea ice depends on the distance to the jet, as argued by Kidston et al. (2011) for the Southern Hemisphere. However, the physical mechanism for this is unclear, especially since differences in jet latitude

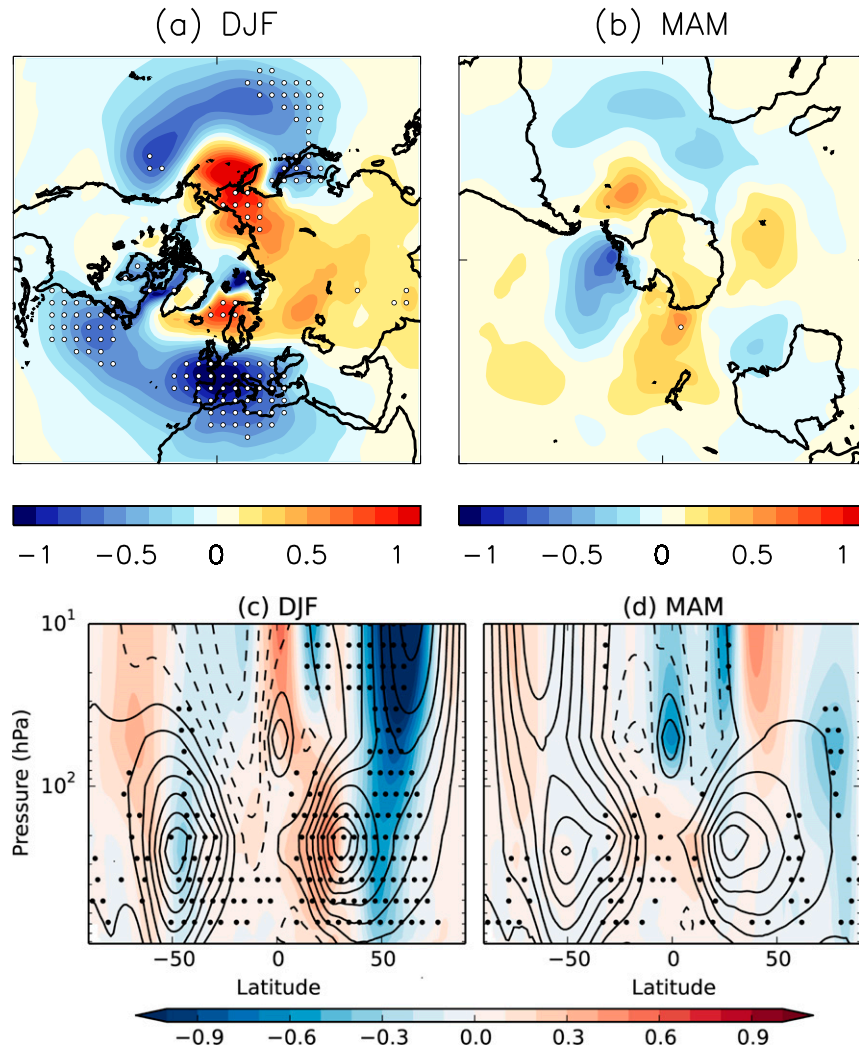


FIG. 10. As in Figs. 5 and 8, but for AMIP_CPLD simulations of (a),(b) mean sea level pressure (hPa) in DJF and MAM and (c),(d) zonal mean zonal wind (m s^{-1}) as a function of latitude and height (in pressure coordinates) for DJF and MAM, respectively. Contours show the AMIP climatological zonal winds (contour interval 5 m s^{-1} ; negative contours are dashed).

between simulations are small compared to the distance between the jet and the sea ice edge. Furthermore, the response also appears to depend on the strength of the jet (Fig. 11b), suggesting that other properties of the background state rather than simply the proximity to the ice edge could be the underlying reason the different responses.

We investigate further by examining the planetary wave response, diagnosed from Eliassen–Palm (EP) fluxes (e.g., Edmon et al. 1980). The zonal-mean zonal flow is accelerated (decelerated) where there is divergence (convergence) of the EP flux. On average, planetary waves originate near the surface in the storm tracks between latitudes 30° and 70°N (red shading in Fig. 12a). They propagate vertically into the stratosphere and are

refracted equatorward, especially in the troposphere (e.g., Li et al. 2007). At midlatitudes, zonal winds are on average accelerated by a divergence of EP flux near the surface and decelerated by a convergence of EP flux in the midtroposphere (shading in Fig. 12e).

In response to reduced Arctic sea ice all three experiments exhibit a reduction in DJF vertical EP flux near the surface, especially between 50° and 60°N , (blue shading near the surface in Figs. 12b–d). This is consistent with reduced Eady growth rates (Eady 1949) in the Gulf Stream and Kuroshio regions (not shown) and can be understood as a weakening of the baroclinic eddy wave source in response to a weaker equator-to-pole surface temperature gradient with reduced ice. Other studies show a similar reduction in wave fluxes

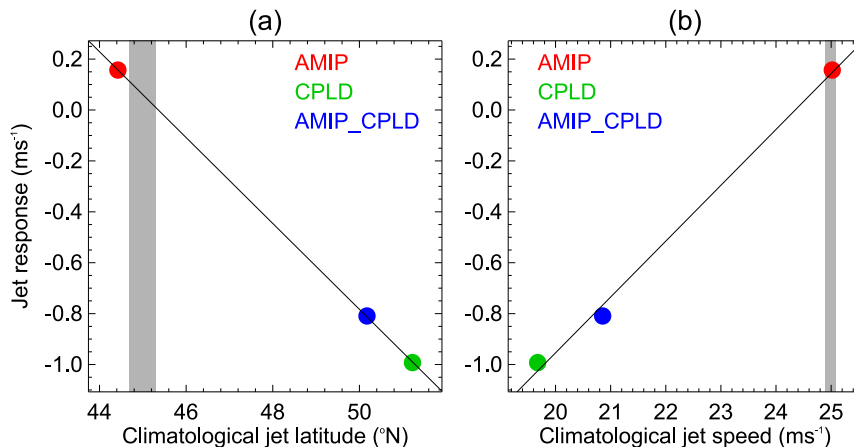


FIG. 11. Dependence of Atlantic jet response on the background climatological flow. (a) Difference in Atlantic eddy driven jet (zonal wind at 200 hPa over the region 50°–60°N, 60°–0°W) between perturbed ice and control experiments as a function of climatological eddy-driven jet latitude diagnosed from the control simulations of the AMIP, CPLD, and AMIP_CPLD experiments. (b) As in (a), but as a function of climatological jet speed. Gray shading shows the observed ranges of jet latitude and strength from ERA-Interim (Dee et al. 2011) and NCEP II (Kanamitsu et al. 2002), using DJF data from 1979 to 2009. Correlations are significant ($p < 0.05$) in both panels.

(Seierstad and Bader 2009; Smith and Scott 2016). However, some studies (Jaiser et al. 2013; Kim et al. 2014; Peings and Magnusdottir 2014; Feldstein and Lee 2014; Sun et al. 2015; Nakamura et al. 2015; Overland et al. 2016) argue that increased vertical EP fluxes, particularly in individual months or in certain regions, are important for driving a negative NAO. While we do find increased vertical EP fluxes in individual months (not shown), and in the high-latitude (70°–80°N) upper troposphere and stratosphere in AMIP and CPLD for DJF (Figs. 12b,c), they are not consistent with the differences in NAO response in the three sets of simulations: for example, the increases at high latitudes occur in both CPLD and AMIP but the NAO response is opposite. Increased vertical EP fluxes are therefore likely to be secondary effects in our simulations.

Although the vertical EP flux source near the surface is reduced in all experiments, the response at higher levels in the atmosphere is different. In particular, there is a convergence (divergence) of EP flux on the poleward (equatorward) flank of the tropospheric jet in both CPLD and AMIP_CPLD, whereas AMIP shows broadly the opposite though the convergence on the equatorward side of the jet is not significant (shading in Figs. 12f–h). Hence, wave forcing acts to shift the tropospheric jet equatorward (poleward) in CPLD and AMIP_CPLD (AMIP), consistent with a negative (positive) NAO response. A possible explanation for the different behavior is therefore that the different background states cause waves to propagate differently.

We investigate further by considering the dependence of the jet response on the climatological refractive index n_k^2 (e.g., Li et al. 2007):

$$n_k^2 = \frac{\bar{q}_\phi}{\bar{u}} - \left(\frac{k}{a \cos \phi} \right)^2 - \left(\frac{f}{2NH} \right)^2, \quad (1)$$

where

$$\bar{q}_\phi = \frac{2\Omega}{a} \cos \phi - \frac{1}{a^2} \left[\frac{(\bar{u} \cos \phi)_\phi}{\cos \phi} \right]_\phi - \frac{f^2}{\rho_0} \left(\rho_0 \frac{\bar{u}_z}{N^2} \right)_z \quad (2)$$

is the meridional gradient of the zonal mean potential vorticity, and k , N , H , f , a , Ω , and ϕ denote the zonal wavenumber, buoyancy frequency, scale height, Coriolis parameter, Earth radius, Earth rotation frequency, and latitude, respectively. Note that waves are refracted toward high values of n_k^2 (e.g., Matsuno 1970; Li et al. 2007).

The reason for the different responses in our simulations is easiest to illustrate by considering the propagation of waves away from an anomalous source. This would be the case for *increased* Arctic sea ice, which drives an *increase* in the Atlantic eddy-driven jet in CPLD and AMIP_CPLD but not in AMIP (as shown in Fig. 11 but with the sign of the response reversed). To understand these differences we compare the response in the jet across the three sets of simulations with the corresponding climatological refractive index and with the response in EP fluxes and divergence. Although

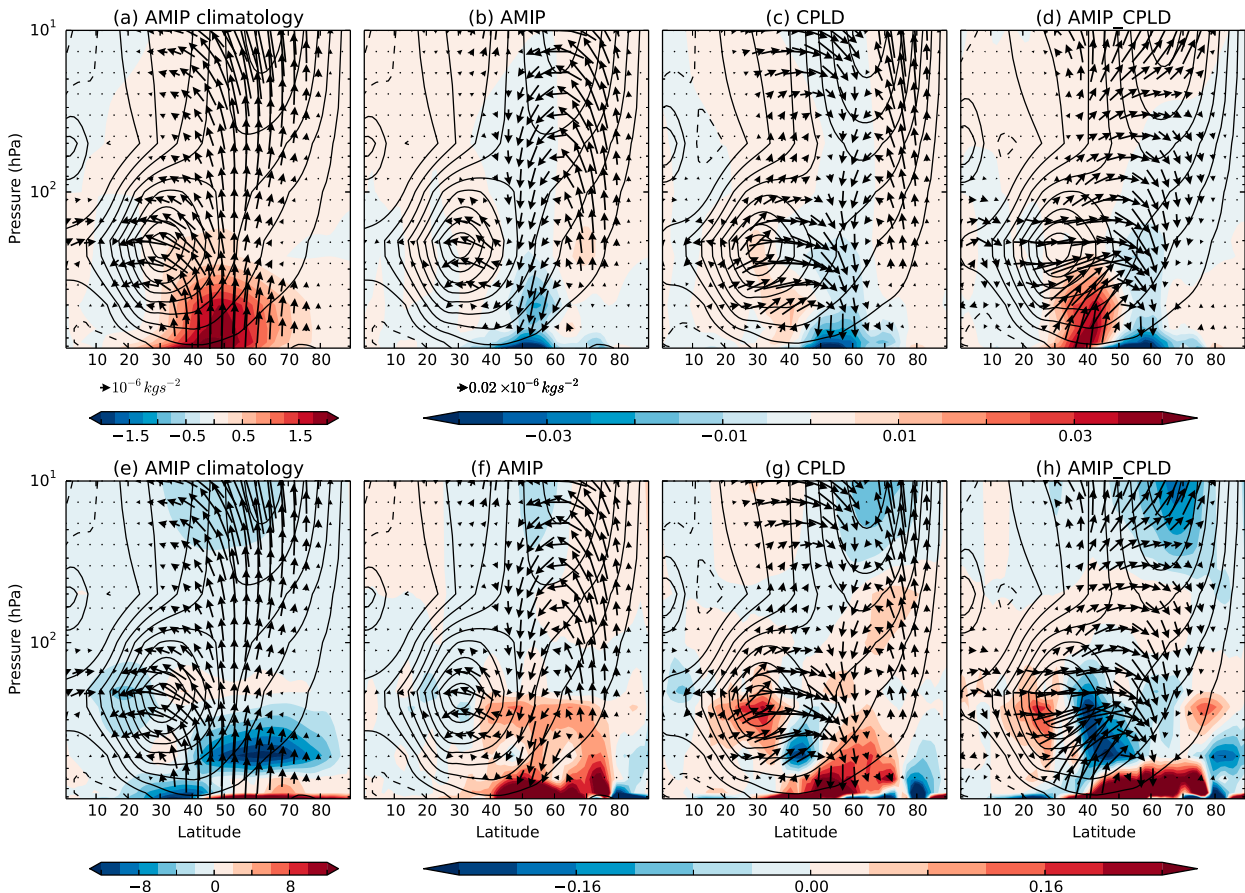


FIG. 12. Northern Hemisphere DJF planetary waves as a function of latitude and height (pressure) in (a),(e) AMIP climatology, and the response to reduced sea ice in (b),(f) AMIP (c),(g) CPLD, and (d),(h) AMIP_CPLD. Color shading shows (top) the vertical EP flux ($10^{-6} \text{ kg s}^{-2}$) and (bottom) the EP flux divergence ($\text{m s}^{-1} \text{ day}^{-1}$). Arrows show the EP flux vector (scaled by dividing by density to aid visualization). Arrow lengths of $10^{-6} \text{ kg s}^{-2}$ for climatology and $0.02 \times 10^{-6} \text{ kg s}^{-2}$ for response are indicated. Black contours show climatological winds (contour interval 5 m s^{-1} ; negative contours are dashed).

there are just three sets of simulations, the large-scale patterns (Fig. 13) suggest that differences in the climatological refractive index potentially explain the different responses. Specifically, a strengthening of the Atlantic jet is associated with an increased equatorward wave flux in the troposphere (Fig. 13, arrows), which interacts with the mean flow associated with the tropospheric jet, resulting in increased EP flux divergence (convergence) on the poleward (equatorward) side of the jet (Fig. 13a). Since EP flux divergence (convergence) accelerates (decelerates) the flow, this is consistent with a poleward shift of the jet and a positive NAO. The role of the background climatological state can now be understood by considering the relation between the jet response and the climatological refractive index (Fig. 13b): since waves tend to be refracted toward higher values of the refractive index (e.g., Matsumo 1970; Li et al. 2007), increased equatorward wave flux in the troposphere is consistent with stronger refraction of

waves toward a climatological refractive index that is higher in midlatitudes (positive correlations shown by red shading) and lower at high latitudes (negative correlations shown by blue shading).

6. What is the NAO response in reality?

Our results imply a central role for the refractive index in determining the Northern Hemisphere winter response to Arctic sea ice. This is consistent with modeled sensitivity to climate change (Sigmond and Scinocca 2010) and with the mechanism proposed by Simpson et al. (2012) to explain the dependence of jet response on its climatological latitude (Son et al. 2010, Kidston and Gerber 2010). A key challenge now is to quantify the response of the real world.

One approach is to use “emergent constraints” (e.g., Collins et al. 2012) in which modeled uncertainties may be reduced by using observations of a quantity

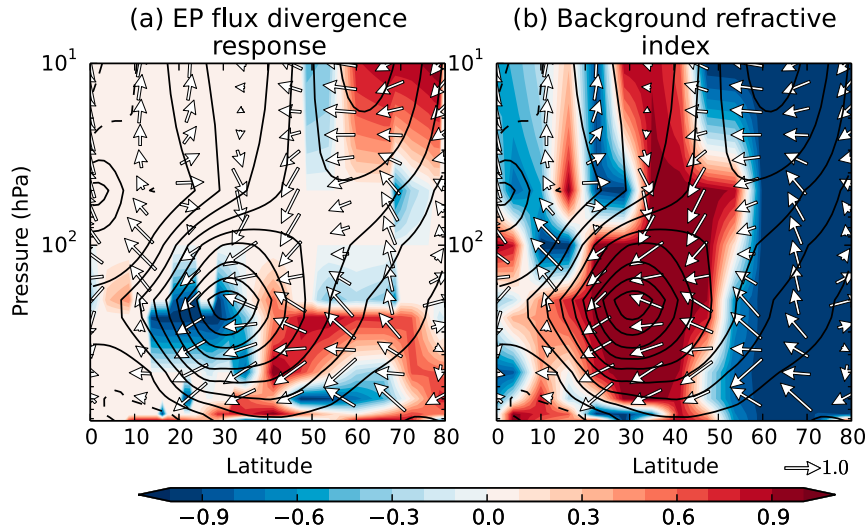


FIG. 13. Correlation across the AMIP, AMIP_CPLD, and CPLD experiments between the response in the Atlantic eddy-driven jet speed to increased Arctic sea ice (as in Fig. 11 but with the sign reversed) and (a) the response in EP flux divergence, and (b) the climatological refractive index for DJF (color shading). Arrows show the correlations between the response in the Atlantic jet and the response in vertical and meridional EP fluxes, plotted as a vector (arrow length for a meridional EP flux correlation of one is indicated). Black contours show the climatological zonal wind for AMIP.

that is correlated across the range of model responses. Observations of the latitude and strength of the Atlantic eddy-driven jet would suggest little response in reality, in closer agreement with AMIP than CPLD (Fig. 11). However, this approach can lead to spurious conclusions (Bracegirdle and Stephenson 2013), particularly if the constraint does not capture the underlying physical mechanism responsible for the model spread (Scaife et al. 2009). The underlying mechanism in our simulations is differences in wave propagation caused by differences in tropospheric refractive index between mid and high latitudes (Fig. 13). A constraint based on refractive index difference is therefore likely to be more realistic than one based on the jet position or strength, and provides further evidence for a negative NAO response to reduced Arctic sea ice (Fig. 14). We note that the refractive index differences between the experiments are dominated by the meridional gradient of the zonal mean potential vorticity, and it is the high-latitude refractive index that is inaccurately simulated in AMIP (not shown), leading to the different constraints in Figs. 11 and 14. Understanding the reason for this is left for future work. Furthermore, we caution that the signal-to-noise ratio in seasonal predictions of the NAO appears to be unrealistically small (Eade et al. 2014, Scaife et al. 2014, Dunstone et al. 2016), so that the magnitude of the response could be larger than simulated by our model.

7. Regression versus true response

Many studies have attempted to assess the impact of Arctic sea ice on the atmospheric circulation from the observations, using statistical analysis usually based on

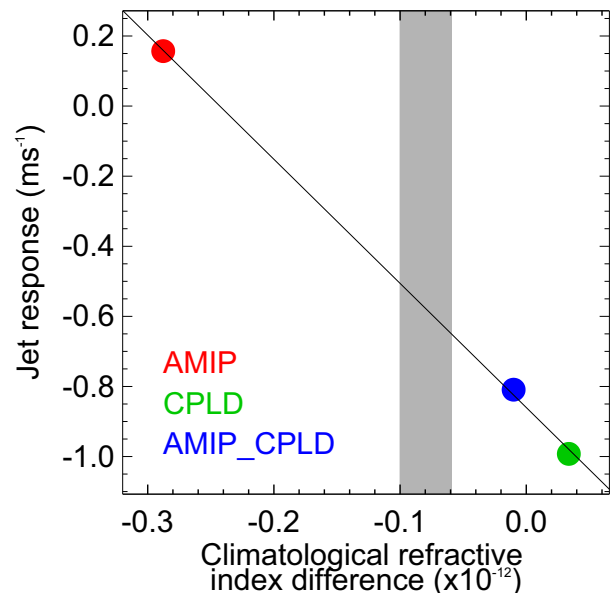


FIG. 14. Dependence of Atlantic jet response on the background climatological refractive index difference between middle (25° – 35°N) and high (60° – 80°N) latitudes at 200 hPa. Gray shading shows the observed range from ERA-Interim and NCEP II.

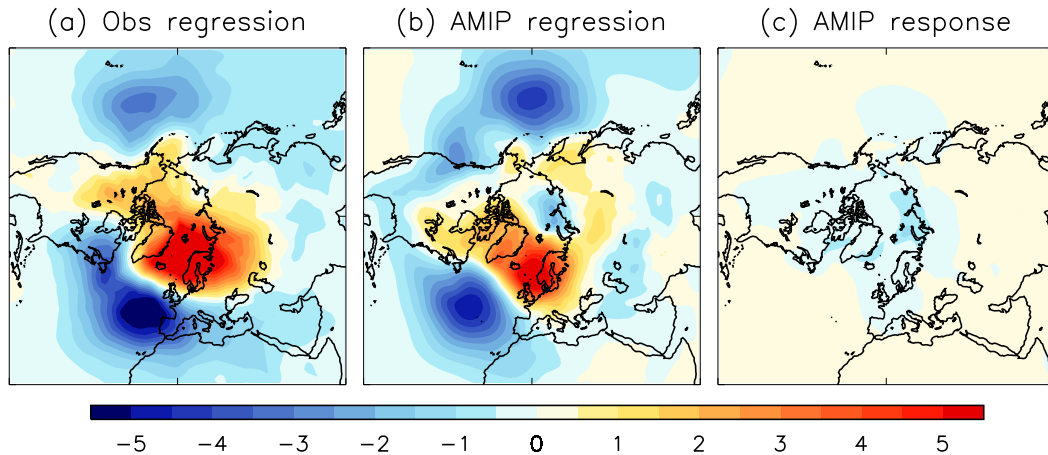


FIG. 15. Inability to determine the response from regression analysis. Linear regression between autumn (SON) Arctic sea ice extent and winter (DJF) mean sea level pressure (reversed sign) in (a) observations (b) AMIP. All time series were linearly detrended. (c) DJF mean sea level response to reduced sea ice in AMIP scaled by the average SON sea ice extent reduction. Units are hPa per million km^2 .

regression or composites (e.g., Overland and Wang 2010; Liu et al. 2012; Tang et al. 2013; Jaiser et al. 2013; Kim et al. 2014; Feldstein and Lee 2014; Francis and Vavrus 2015; Handorf et al. 2015; Kug et al. 2015; Luo et al. 2016; Yang et al. 2016). However, causality cannot be inferred from statistical relationships, and this approach may give misleading results when other factors are important. We illustrate this by computing the linear regression between autumn (SON) Arctic sea ice extent and the following winter (DJF) mean sea level pressure. A lag is required to avoid the contemporaneous impact of the atmospheric circulation on the sea ice, and assumes that sea ice in SON drives a response that propagates through the climate system to influence the DJF sea level pressure. Both observed and AMIP regressions show a negative NAO pattern (Figs. 15a,b), suggesting that reduced Arctic sea ice loss could be driving a negative NAO. However, the actual response to Arctic sea ice in the AMIP simulations is very different from that suggested by the regression analysis, with a very weak positive NAO (Fig. 15c). Similar analysis of the CPLD experiments also shows a different response from that diagnosed from regression (not shown). Hence, although statistical analysis can give some insight in some cases, it can also give misleading results. Statistical analysis must therefore be interpreted with caution, and model experiments are needed to assess causality.

8. Summary and conclusions

We have performed a comprehensive set of model experiments to assess the atmospheric impact of Arctic

and Antarctic sea ice changes typical of the present day and near future. The experiments enable the roles of ocean–atmosphere coupling and the climatological background state of the atmosphere to be assessed. We show that the response inferred from statistical relationships may be opposite to the true response due to confounding factors. Hence, the response cannot easily be inferred from the observations, despite many attempts in the literature.

In boreal summer and autumn sea level pressure reduces over the Arctic consistent with a heat low response to warmer surface temperatures. This response is larger in the coupled simulations, which have greater surface warming. Precipitation increases significantly over the Arctic in SON. However, hypothesized increases in Eurasian snow cover (Cohen et al. 2012) are not simulated by our model, in agreement with Sun et al. (2015). Further studies are needed to assess this potential linkage.

The response to increased Antarctic sea ice shows a poleward shift of the midlatitude tropospheric jet in the cold seasons consistent with previous studies (Simmonds and Budd 1991; Menéndez et al. 1999; Kidston et al. 2011; Bader et al. 2013). However, further work is required to assess the response to projected future decreases in Antarctic sea ice, for which Bader et al. (2013) find an equatorward shift of the jet but Kidston et al. (2011) find little response, arguing that ice edge becomes too far away to influence the jet. However, our results for the Northern Hemisphere jet (summarized below) highlight the importance of the background state rather than the distance to the ice edge, and might help to explain the difference in these two studies.

Coupling enables surface temperature responses to spread to the ocean (Deser et al. 2015, 2016; Tomas et al. 2016). In our model, reduced Arctic sea ice drives a warmer North Atlantic especially in boreal summer and autumn, leading to increased Sahel rainfall comparable in magnitude to long-term projections in response to greenhouse gases (Biasutti 2013). This is consistent with Chiang and Bitz (2005) but does not appear to be simulated in some other studies (Deser et al. 2015; Tomas et al. 2016). Further work is needed to understand the reason for these differences.

Our main focus is on the boreal winter NAO, for which previous results are controversial (Wallace et al. 2014). The sign of the NAO response to reduced Arctic sea ice depends on the climatological background state in our model. The overall response consists of a thermodynamic heat low projecting onto a positive NAO, together with a dynamical weakening of the westerly flow which projects onto a negative NAO. Whether the dynamical weakening dominates, giving a negative NAO overall, depends on the propagation of planetary waves, which is governed by the climatological refractive index and in particular its difference between the middle and high latitudes.

The mechanism for the NAO response is different from many studies that highlight an increase in planetary wave activity in response to reduced Arctic sea ice (Jaiser et al. 2013; Kim et al. 2014; Peings and Magnusdottir 2014; Feldstein and Lee 2014; Sun et al. 2015; Nakamura et al. 2015; Overland et al. 2016). Instead, we find that reduced Arctic sea ice drives a reduction in upward planetary waves from the surface. This is in agreement with some previous studies (Seierstad and Bader 2009, Smith and Scott 2016) and can be understood as a weakening of the baroclinic-eddy wave source in response to a weaker equator to pole surface temperature gradient. The impact on the tropospheric jet (and hence the NAO) is easier to illustrate by considering the case of increased Arctic sea ice. This drives an increase in upward planetary waves, which are refracted equatorward in the troposphere. They converge (diverge) on the equatorward (poleward) flank of the jet, leading to poleward shift and a positive NAO (negative for reduced sea ice). The magnitude of this response is governed by the amount of equatorward refraction of planetary waves, and hence depends on the background refractive index.

The importance of the background state for the NAO response could help to resolve some of the differences seen in previous studies, and potentially provides an “emergent constraint” to reduce the uncertainties. In our simulations, an emergent constraint based on the observed difference in upper tropospheric refractive

index between the middle and high latitudes provides further support for a negative NAO response to reduced Arctic sea ice in reality. However, our results are with a single model and a single experimental design, whereas differences found in previous studies might be caused by different models, forcings, and experimental setups. Hence, multimodel coordinated experiments are required to isolate these different factors, and to provide a more robust constraint on the likely real-world response to Arctic sea ice loss. Finally, we note that although the simulated NAO response is quite weak (less than 80% of its interannual standard deviation), the magnitude could be incorrect given that the signal-to-noise ratio in climate predictions of the NAO is too small (Eade et al. 2014; Scaife et al. 2014). Further work is needed to resolve this issue.

Acknowledgments. This work was supported by the joint DECC/Defra Met Office Hadley Centre Climate Programme (GA01101), and the EU FP7 SPECS and H2020 APPLICATE projects. ECMWF ERA-Interim data used in this study have been obtained from the ECMWF data server. NCEP reanalyses were obtained from the NOAA-ESRL Physical Sciences Division, Boulder Colorado from their Web site at <http://www.esrl.noaa.gov/psd/>. We thank Professor James Screen and two anonymous reviewers for their thoughtful comments.

REFERENCES

- Alexander, M. A., U. S. Bhatt, J. E. Walsh, M. S. Timlin, J. S. Miller, and J. D. Scott, 2004: The atmospheric response to realistic Arctic sea ice anomalies in an AGCM during winter. *J. Climate*, **17**, 890–905, doi:10.1175/1520-0442(2004)017<0890:TARTRA>2.0.CO;2.
- Bader, J., M. Flügge, N. G. Kvamstø, M. D. S. Mesquita, and A. Voigt, 2013: Atmospheric winter response to a projected future Antarctic sea-ice reduction: A dynamical analysis. *Climate Dyn.*, **40**, 2707–2718, doi:10.1007/s00382-012-1507-9.
- Barnes, E. A., and J. A. Screen, 2015: The impact of Arctic warming on the midlatitude jet-stream: Can it? Has it? Will it? *Climatic Change*, **6**, 277–286, doi:10.1002/wcc.337.
- Biasutti, M., 2013: Forced Sahel rainfall trends in the CMIP5 archive. *J. Geophys. Res. Atmos.*, **118**, 1613–1623, doi:10.1002/jgrd.50206.
- Blackport, R., and P. Kushner, 2016: The transient and equilibrium climate response to rapid summertime sea ice loss in CCSM4. *J. Climate*, **29**, 401–417, doi:10.1175/JCLI-D-15-0284.1.
- Bracegirdle, T. J., and D. B. Stephenson, 2013: On the robustness of emergent constraints used in multimodel climate change projections of Arctic warming. *J. Climate*, **26**, 669–678, doi:10.1175/JCLI-D-12-00537.1.
- Cassano, E. N., J. J. Cassano, M. E. Higgins, and M. C. Serreze, 2014: Atmospheric impacts of an Arctic sea ice minimum as seen in the Community Atmosphere Model. *Int. J. Climatol.*, **34**, 766–779, doi:10.1002/joc.3723.
- Chiang, J. C. H., and C. M. Bitz, 2005: Influence of high latitude ice cover on the marine intertropical convergence zone. *Climate Dyn.*, **25**, 477–496, doi:10.1007/s00382-005-0040-5.

- Cohen, J., J. Furtado, J. M. Barlow, V. Alexeev, and J. Cherry, 2012: Arctic warming, increasing fall snow cover and widespread boreal winter cooling. *Environ. Res. Lett.*, **7**, 014007, doi:10.1088/1748-9326/7/1/014007.
- , and Coauthors, 2014: Recent Arctic amplification and extreme mid-latitude weather. *Nat. Geosci.*, **7**, 627–637, doi:10.1038/ngeo2234.
- Collins, M., R. E. Chandler, P. M. Cox, J. M. Huthnance, J. Rougier, and D. B. Stephenson, 2012: Quantifying future climate change. *Nat. Climate Change*, **2**, 403–409, doi:10.1038/nclimate1414.
- , and Coauthors, 2013: Long-term climate change: Projections, commitments and irreversibility. *Climate Change 2013: The Physical Science Basis*, T. F. Stocker et al., Eds., Cambridge University Press, 1029–1136.
- Dee, D. P., and Coauthors, 2011: The ERA-Interim reanalysis: Configuration and performance of the data assimilation system. *Quart. J. Roy. Meteor. Soc.*, **137**, 553–597, doi:10.1002/qj.828.
- Deser, C., G. Magnusdottir, R. Saravanan, and A. Phillips, 2004: The effects of North Atlantic SST and sea ice anomalies on the winter circulation in CCM3. Part II: Direct and indirect components of the response. *J. Climate*, **17**, 877–889, doi:10.1175/1520-0442(2004)017<0877:TEONAS>2.0.CO;2.
- , R. A. Tomas, and L. Sun, 2015: The role of ocean–atmosphere coupling in the zonal-mean atmospheric response to Arctic sea ice loss. *J. Climate*, **28**, 2168–2186, doi:10.1175/JCLI-D-14-00325.1.
- , L. Sun, R. A. Tomas, and J. Screen, 2016: Does ocean coupling matter for the northern extra-tropical response to projected Arctic sea ice loss? *Geophys. Res. Lett.*, **43**, 2149–2157, doi:10.1002/2016GL067792.
- Dunstone, N. J., and D. M. Smith, 2010: Impact of atmosphere and sub-surface ocean data on decadal climate prediction. *Geophys. Res. Lett.*, **37**, L02709, doi:10.1029/2009GL041609.
- , —, and R. Eade, 2011: Multi-year predictability of the tropical Atlantic atmosphere driven by the high latitude north Atlantic Ocean. *Geophys. Res. Lett.*, **38**, L14701, doi:10.1029/2011GL047949.
- , —, A. A. Scaife, L. Hermanson, R. Eade, N. Robinson, M. Andrews, and J. Knight, 2016: Skilful predictions of the winter North Atlantic Oscillation one year ahead. *Nat. Geosci.*, **9**, 809–814, doi:10.1038/ngeo2824.
- Eade, R., D. M. Smith, A. A. Scaife, E. Wallace, N. Dunstone, L. Hermanson, and N. Robinson, 2014: Do seasonal-to-decadal climate predictions underestimate the predictability of the real world? *Geophys. Res. Lett.*, **41**, 5620–5628, doi:10.1002/2014GL061146.
- Eady, E., 1949: Long waves and cyclone waves. *Tellus*, **1**, 33–52, doi:10.3402/tellusa.v1i3.8507.
- Edmon, H. J., Jr., B. J. Hoskins, and M. E. McIntyre, 1980: Eliassen–Palm cross sections for the troposphere. *J. Atmos. Sci.*, **37**, 2600–2616, doi:10.1175/1520-0469(1980)037<2600:EPCSFT>2.0.CO;2.
- Feldstein, S., and S. Lee, 2014: Intraseasonal and interdecadal jet shifts in the Northern Hemisphere: The role of warm pool tropical convection and sea ice. *J. Climate*, **27**, 6497–6518, doi:10.1175/JCLI-D-14-00057.1.
- Francis, J. A., and S. J. Vavrus, 2015: Evidence for a wavier jet stream in response to rapid Arctic warming. *Environ. Res. Lett.*, **10**, 014005, doi:10.1088/1748-9326/10/1/014005.
- Garfinkel, C. I., D. W. Waugh, and E. P. Gerber, 2013: The effect of tropospheric jet latitude on coupling between the stratospheric polar vortex and the troposphere. *J. Climate*, **26**, 2077–2095, doi:10.1175/JCLI-D-12-00301.1.
- Goldenberg, S. B., C. W. Landsea, A. M. Mestas-Núñez, and W. M. Gray, 2001: The recent increase in Atlantic hurricane activity: Causes and implications. *Science*, **293**, 474–479, doi:10.1126/science.1060040.
- Gong, D., and S. Wang, 1999: Definition of Antarctic oscillation index. *Geophys. Res. Lett.*, **26**, 459–462, doi:10.1029/1999GL900003.
- Handorf, D., R. Jaiser, K. Dethloff, A. Rinke, and J. Cohen, 2015: Impacts of Arctic sea ice and continental snow cover changes on atmospheric winter teleconnections. *Geophys. Res. Lett.*, **42**, 2367–2377, doi:10.1002/2015GL063203.
- Hardiman, S. C., N. Butchart, T. J. Hinton, S. M. Osprey, and L. J. Gray, 2012: The effect of a well-resolved stratosphere on surface climate: Differences between CMIP5 simulations with high and low top versions of the Met Office climate model. *J. Climate*, **25**, 7083–7099, doi:10.1175/JCLI-D-11-00579.1.
- Honda, M., J. Inoue, and S. Yamane, 2009: Influence of low Arctic sea-ice minima on anomalously cold Eurasian winters. *Geophys. Res. Lett.*, **36**, L08707, doi:10.1029/2008GL037079.
- Hurrell, J. W., 1995: Decadal trends in the North Atlantic Oscillation and relationships to regional temperature and precipitation. *Science*, **269**, 676–679, doi:10.1126/science.269.5224.676.
- , J. J. Hack, D. Shea, J. M. Caron, and J. Rosinski, 2008: A new sea surface temperature and sea ice boundary dataset for the Community Atmosphere Model. *J. Climate*, **21**, 5145–5153, doi:10.1175/2008JCLI2292.1.
- Jaiser, R., K. Dethloff, and D. Handorf, 2013: Stratospheric response to Arctic sea ice retreat and associated planetary wave propagation changes. *Tellus*, **65A**, 19375, doi:10.3402/tellusa.v65i0.19375.
- Kanamitsu, M., W. Ebisuzaki, J. Woollen, S.-K. Yang, J. J. Hnilo, M. Fiorino, and G. L. Potter, 2002: NCEP–DOE AMIP-II Reanalysis (R-2). *Bull. Amer. Meteor. Soc.*, **83**, 1631–1643, doi:10.1175/BAMS-83-11-1631.
- Kang, S. M., I. M. Held, D. M. W. Frierson, and M. Zhao, 2008: The response of the ITCZ to extratropical thermal forcing: Idealized slab-ocean experiments with a GCM. *J. Climate*, **21**, 3521–3532, doi:10.1175/2007JCLI2146.1.
- Kidston, J., and E. P. Gerber, 2010: Intermodel variability of the poleward shift of the austral jet stream in the CMIP3 integrations linked to biases in 20th century climatology. *Geophys. Res. Lett.*, **37**, L09708, doi:10.1029/2010GL042873.
- , A. S. Taschetto, D. W. J. Thompson, and M. H. England, 2011: The influence of Southern Hemisphere sea-ice extent on the latitude of the mid-latitude jet stream. *Geophys. Res. Lett.*, **38**, L15804, doi:10.1029/2011GL048056.
- Kim, B.-M., S.-W. Son, S.-K. Min, J.-H. Jeong, S.-J. Kim, X. Zhang, T. Shim, and J.-H. Yoon, 2014: Weakening of the stratospheric polar vortex by Arctic sea-ice loss. *Nat. Commun.*, **5**, 4646, doi:10.1038/ncomms5646.
- Knight, J. R., R. J. Allan, C. K. Folland, M. Vellinga, and M. E. Mann, 2005: A signature of persistent natural thermohaline circulation cycles in observed climate. *Geophys. Res. Lett.*, **32**, L20708, doi:10.1029/2005GL024233.
- Kug, J.-S., J.-H. Jeong, Y.-S. Jang, B.-M. Kim, C. K. Folland, S.-K. Min, and S.-W. Son, 2015: Two distinct influences of Arctic warming on cold winters over North America and East Asia. *Nat. Geosci.*, **8**, 759–762, doi:10.1038/ngeo2517.
- Li, Q., H. F. Graf, and M. A. Giorgetta, 2007: Stationary planetary wave propagation in Northern Hemisphere winter—Climatological analysis of the refractive index. *Atmos. Chem. Phys.*, **7**, 183–200, doi:10.5194/acp-7-183-2007.

- Liu, J., J. A. Curry, H. Wang, M. Song, and R. M. Horton, 2012: Impact of declining Arctic sea ice on winter snowfall. *Proc. Natl. Acad. Sci. USA*, **109**, 4074–4079, doi:10.1073/pnas.1114910109.
- Luo, D., Y. Xiao, Y. Yao, A. Dai, I. Simmonds, and C. Franzke, 2016: Impact of Ural blocking on winter warm Arctic–cold Eurasian anomalies. Part I: Blocking-induced amplification. *J. Climate*, **29**, 3925–3947, doi:10.1175/JCLI-D-15-0611.1.
- Matsumo, T., 1970: Vertical propagation of stationary planetary waves in the winter Northern Hemisphere. *J. Atmos. Sci.*, **27**, 871–883, doi:10.1175/1520-0469(1970)027<0871:VPOSPW>2.0.CO;2.
- Menéndez, C. G., V. Serafini, and H. Le Treut, 1999: The effect of sea-ice on the transient atmospheric eddies of the Southern Hemisphere. *Climate Dyn.*, **15**, 659–671, doi:10.1007/s003820050308.
- Mori, M., M. Watanabe, H. Shiogama, J. Inoue, and M. Kimoto, 2014: Robust Arctic sea-ice influence on the frequent Eurasian cold winters in past decades. *Nat. Geosci.*, **7**, 869–873, doi:10.1038/ngeo2277.
- Nakamura, T., K. Yamazaki, K. Iwamoto, M. Honda, Y. Miyoshi, Y. Ogawa, and J. Ukita, 2015: A negative phase shift of the winter AO/NAO due to the recent Arctic sea-ice reduction in late autumn. *J. Geophys. Res. Atmos.*, **120**, 3209–3227, doi:10.1002/2014JD022848.
- Omrani, N. E., N. S. Keenlyside, J. Bader, and E. Manzini, 2014: Stratosphere key for wintertime atmospheric response to warm Atlantic decadal conditions. *Climate Dyn.*, **42**, 649–663, doi:10.1007/s00382-013-1860-3.
- Orsolini, Y. J., R. Senan, R. E. Benestad, and A. Melsom, 2012: Autumn atmospheric response to the 2007 low Arctic sea ice extent in coupled ocean–atmosphere hindcasts. *Climate Dyn.*, **38**, 2437–2448, doi:10.1007/s00382-011-1169-z.
- Overland, J. E., and M. Wang, 2010: Large-scale atmospheric circulation changes are associated with the recent loss of Arctic sea ice. *Tellus*, **62A**, 1–9, doi:10.1111/j.1600-0870.2009.00421.x.
- , J. Francis, R. Hall, E. Hanna, S. Kim, and T. Vihma, 2015: The melting Arctic and midlatitude weather patterns: Are they connected? *J. Climate*, **28**, 7917–7932, doi:10.1175/JCLI-D-14-00822.1.
- , and Coauthors, 2016: Nonlinear response of mid-latitude weather to the changing Arctic. *Nat. Climate Change*, **6**, 992–999, doi:10.1038/nclimate3121.
- Pedersen, R., I. Cvijanovic, P. Langen, and B. Vinther, 2016: The impact of regional Arctic sea ice loss on atmospheric circulation and the NAO. *J. Climate*, **29**, 889–902, doi:10.1175/JCLI-D-15-0315.1.
- Peings, Y., and G. Magnusdottir, 2014: Response of the wintertime Northern Hemisphere atmospheric circulation to current and projected Arctic sea ice decline: A numerical study with CAM5. *J. Climate*, **27**, 244–264, doi:10.1175/JCLI-D-13-00272.1.
- Petoukhov, V., and V. A. Semenov, 2010: A link between reduced Barents-Kara sea ice and cold winter extremes over northern continents. *J. Geophys. Res.*, **115**, D21111, doi:10.1029/2009JD013568.
- Petrie, R. E., L. C. Shaffrey, and R. T. Sutton, 2015: Atmospheric impact of Arctic sea ice loss in a coupled ocean–atmosphere simulation. *J. Climate*, **28**, 9606–9622, doi:10.1175/JCLI-D-15-0316.1.
- Rácz, Zs., and R. K. Smith, 1999: The dynamics of heat lows. *Quart. J. Roy. Meteor. Soc.*, **125**, 225–252, doi:10.1002/qj.49712555313.
- Rinke, A., K. Dethloff, W. Dorn, D. Handorf, and J. C. Moore, 2013: Simulated Arctic atmospheric feedbacks associated with late summer sea ice anomalies. *J. Geophys. Res. Atmos.*, **118**, 7698–7714, doi:10.1002/jgrd.50584.
- Scaife, A. A., and Coauthors, 2014: Skillful long range prediction of European and North American winters. *Geophys. Res. Lett.*, **41**, 2514–2519, doi:10.1002/2014GL059637.
- , C. Buontempo, M. Ringer, M. Sanderson, C. Gordon, and J. Mitchell, 2009: Toward seamless prediction: Calibration of climate change projections using seasonal forecasts. *Bull. Amer. Meteor. Soc.*, **90**, 1549–1551, doi:10.1175/2009BAMS2753.1.
- Screen, J. A., I. Simmonds, C. Deser, and R. Tomas, 2013: The atmospheric response to three decades of observed Arctic sea ice loss. *J. Climate*, **26**, 1230–1248, doi:10.1175/JCLI-D-12-00063.1.
- , C. Deser, I. Simmonds, and R. Tomas, 2014: Atmospheric impacts of Arctic sea-ice loss, 1979–2009: Separating forced change from atmospheric internal variability. *Climate Dyn.*, **43**, 333–344, doi:10.1007/s00382-013-1830-9.
- Seierstad, I., and J. Bader, 2009: Impact of a projected future Arctic sea ice reduction on extratropical storminess and the NAO. *Climate Dyn.*, **33**, 937–943, doi:10.1007/s00382-008-0463-x.
- Sheen, K. L., D. M. Smith, N. J. Dunstone, R. Eade, D. P. Rowell, and M. Vellinga, 2017: Skillful prediction of Sahel summer rainfall on interannual and multiyear timescales. *Nat. Commun.*, in press.
- Sigmond, M., and J. F. Scinocca, 2010: The influence of the basic state on the Northern Hemisphere circulation response to climate change. *J. Climate*, **23**, 1434–1446, doi:10.1175/2009JCLI3167.1.
- Simmonds, I., and W. F. Budd, 1991: Sensitivity of the Southern Hemisphere circulation to leads in the Antarctic pack ice. *Quart. J. Roy. Meteor. Soc.*, **117**, 1003–1024, doi:10.1002/qj.49711750107.
- , and X. Wu, 1993: Cyclone behaviour response to changes in winter Southern Hemisphere sea-ice concentration. *Quart. J. Roy. Meteor. Soc.*, **119**, 1121–1148, doi:10.1002/qj.49711951313.
- Simpson, I. R., M. Blackburn, and J. D. Haigh, 2012: A mechanism for the effect of tropospheric jet structure on the annular mode–like response to stratospheric forcing. *J. Atmos. Sci.*, **69**, 2152–2170, doi:10.1175/JAS-D-11-0188.1.
- Singarayer, J. S., J. L. Bamber, and P. J. Valdes, 2006: Twenty-first-century climate impacts from a declining Arctic sea ice cover. *J. Climate*, **19**, 1109–1125, doi:10.1175/JCLI3649.1.
- Smith, D. M., R. Eade, N. J. Dunstone, D. Fereday, J. M. Murphy, H. Pohlmann, and A. A. Scaife, 2010: Skillful multi-year predictions of Atlantic hurricane frequency. *Nat. Geosci.*, **3**, 846–849, doi:10.1038/ngeo1004.
- , —, and H. Pohlmann, 2013: A comparison of full-field and anomaly initialization for seasonal to decadal climate prediction. *Climate Dyn.*, **41**, 3325–3338, doi:10.1007/s00382-013-1683-2.
- , and Coauthors, 2015: Earth’s energy imbalance since 1960 in observations and CMIP5 models. *Geophys. Res. Lett.*, **42**, 1205–1213, doi:10.1002/2014GL062669.
- Smith, K. L., and R. K. Scott, 2016: The role of planetary waves in the tropospheric jet response to stratospheric cooling. *Geophys. Res. Lett.*, **43**, 2904–2911, doi:10.1002/2016GL067849.
- Son, S.-W., and Coauthors, 2010: Impact of stratospheric ozone on Southern Hemisphere circulation change: A multimodel assessment. *J. Geophys. Res.*, **115**, D00M07, doi:10.1029/2010JD014271.
- Strey, S. T., W. L. Chapman, and J. E. Walsh, 2010: The 2007 sea ice minimum: Impacts on the Northern Hemisphere atmosphere in late autumn and early winter. *J. Geophys. Res.*, **115**, D23103, doi:10.1029/2009JD013294.
- Sun, L., C. Deser, and R. A. Tomas, 2015: Mechanisms of stratospheric and tropospheric circulation response to projected Arctic sea ice loss. *J. Climate*, **28**, 7824–7845, doi:10.1175/JCLI-D-15-0169.1.

- Tang, Q., X. Zhang, X. Yang, and J. A. Francis, 2013: Cold winter extremes in northern continents linked to Arctic sea ice loss. *Environ. Res. Lett.*, **8**, 014036, doi:[10.1088/1748-9326/8/1/014036](https://doi.org/10.1088/1748-9326/8/1/014036).
- Tomas, R. A., C. Deser, and L. Sun, 2016: The role of ocean heat transport in the global climate response to projected Arctic sea ice loss. *J. Climate*, **29**, 6841–6859, doi:[10.1175/JCLI-D-15-0651.1](https://doi.org/10.1175/JCLI-D-15-0651.1).
- Vaughan, D. G., and Coauthors, 2013: Observations: Cryosphere. *Climate Change 2013: The Physical Science Basis*, T. F. Stocker et al., Eds., Cambridge University Press, 317–382.
- Vihma, T., 2014: Effects of Arctic sea ice decline on weather and climate: A review. *Surv. Geophys.*, **35**, 1175–1214, doi:[10.1007/s10712-014-9284-0](https://doi.org/10.1007/s10712-014-9284-0).
- Wallace, J. M., I. M. Held, D. W. J. Thompson, K. E. Trenberth, and J. E. Walsh, 2014: Global warming and winter weather. *Science*, **343**, 729–730, doi:[10.1126/science.1243.6172.729](https://doi.org/10.1126/science.1243.6172.729).
- Walsh, J. E., 2014: Intensified warming of the Arctic: Causes and impacts on middle latitudes. *Global Planet. Change*, **117**, 52–63, doi:[10.1016/j.gloplacha.2014.03.003](https://doi.org/10.1016/j.gloplacha.2014.03.003).
- Walters, D. N., and Coauthors, 2011: The Met Office Unified Model Global Atmosphere 3.0/3.1 and JULES Global Land 3.0/3.1 configurations. *Geosci. Model Dev.*, **4**, 919–941, doi:[10.5194/gmd-4-919-2011](https://doi.org/10.5194/gmd-4-919-2011).
- Yang, X.-Y., Y. Yuan, and M. Ting, 2016: Dynamical link between the Barents–Kara sea ice and the Arctic Oscillation. *J. Climate*, **29**, 5103–5122, doi:[10.1175/JCLI-D-15-0669.1](https://doi.org/10.1175/JCLI-D-15-0669.1).